Modulated Self-Assembly of an Interpenetrated MIL-53 Sc Metal-Organic Framework with Excellent Volumetric H_2 Storage and Working Capacity

Alexander J. R. Thom,[a] David G. Madden,[b] Rocio Bueno-Perez,[b] Ali N. Al Shakhs,[b] Ciaran T. Lennon,[a] Ross J. Marshall,[a] Claire Wilson,[a] Claire A. Murray,[c] Stephen P. Thompson,[c] Gemma F. Turner,[d] Dominic Bara,[a] Stephen A. Moggach,[d] David Fairen-Jimenez[b*] and Ross S. Forgan[a*]

[a]WestCHEM School of Chemistry, University of Glasgow, Joseph Black Building, University Avenue, Glasgow G12 8QQ, UK.
Email: ross.forgan@glasgow.ac.uk

[b]The Adsorption & Advanced Materials Laboratory (A^2ML), Department of Chemical Engineering & Biotechnology, University of Cambridge, Philippa Fawcett Drive, Cambridge CB3 0AS, UK.
Email: df334@cam.ac.uk

[c]Diamond Light Source Ltd, Harwell Science and Innovation Campus, Didcot, Oxfordshire OX11 0DE, UK.

[d]School of Molecular Sciences, The University of Western Australia, 35 Stirling Highway, Crawley, Perth, Western Australia, 6009, Australia.

Abstract

To achieve optimal performance in gas storage and delivery applications, metal-organic frameworks (MOFs) must combine high gravimetric and volumetric capacities. One potential route to balancing high pore volume with suitable crystal density is interpenetration, where identical nets sit within the void space of one another. Herein, we report an interpenetrated MIL-53 topology MOF, named GUF-1, where one-dimensional Sc(μ_2-OH) chains are connected by 4,4′-(ethyne-1,2-diyl)dibenzoate linkers into a material that is an unusual example of an interpenetrated MOF with a rod-like secondary building unit. A combination of modulated self-assembly and grand canonical Monte Carlo simulations are used to optimise the porosity of GUF-1; H_2 adsorption isotherms reveal a very high Q_{st} for H_2 of 7.6 kJ mol^{-1} and a working capacity of 41 g L^{-1} in a temperature-pressure swing system, which is comparable to benchmark MOFs. These results show that interpenetration is a viable route to high performance gas storage materials comprised of relatively simple building blocks.

Introduction

Metal-organic frameworks (MOFs) are network solids wherein metal ions or clusters are connected by organic ligands into extended structures.[1] A number of MOFs have been proposed as potential gas capture and separation materials,[2-7] including candidates for H_2 storage applications,[8-15] due to their prodigious storage capacities and ease of structure optimisation and functionalisation. To enhance adsorption capacity, the isoreticular principle[16] – extending the linker length whilst maintaining the metal secondary building unit (SBU) and topology – is often applied.[17] This strategy can enhance pore volume, but interpenetration of multiple nets within the pore space of each other can result in reduced overall uptake, albeit sometimes enhancing substrate selectivity.[18-21] MOFs with topologies that exclude the possibility of interpenetration,[22] as well as bespoke synthetic techniques,[23] can also be used to maximise pore volume. At the same time, the main challenge to improve volumetric H_2 storage capacity is maximizing density as well as gas uptake.[5, 24] Indeed, while many studies have previously focused on MOFs with high gravimetric BET areas and pore volumes, the high gravimetric H_2 adsorption capacities did not readily translate to high volumetric H_2 adsorption performance due to the low framework densities of these materials.[25] Recently, the development of MOFs for H_2 storage has focused on materials which balance gravimetric and volumetric adsorption performance, whereby MOFs combining optimal pore volumes and structural density give way to materials with exceptional volumetric BET areas.[8, 11, 26, 27] While many of these MOFs display exceptional H_2 adsorption performance, they often contain complex organic linker ligands and/or complex synthesis procedures.[11] As such, accessing interpenetrated analogues of archetypal MOF systems represents a potentially straightforward route to materials with increased volumetric capacities, facilitated by the increase in MOF structural density and simultaneously enhanced adsorbate-adsorbent interactions.[28-30]

Classical MOFs such as those from the MIL family (MIL = Materiaux Institute Lavoisier) have displayed benchmark gas adsorption performance for numerous applications.[31-33] While many MOFs of the MIL family utilise trivalent metals such as Cr^{3+}, Fe^{3+} and Al^{3+}, the use of light trivalent metals such as Sc^{3+} is considerably rarer. There are less than one hundred Sc MOFs and coordination polymers in the Cambridge Structural Database; compared to the 100,000 known MOFs, this is less than 0.1% of the available crystal structures,[34] and only a fraction of these MOFs have been subsequently utilised for hydrogen storage.[35-38] Sc MOFs exhibit SBUs analogous to their more common trivalent transition metal congeners, including the one-dimensional metal hydroxide chain SBU, where each metal is bridged by four carboxylate oxygen donors and two μ_2-OH linkers, as seen in MIL-53(Sc)[39, 40] and MIL-68(Sc),[41] as well as the discrete trimeric $[Sc_3O(RCO_2)_6]$ cluster observed in MIL-101(Sc)[40, 41] and MIL-88B(Sc).[35, 42] A further one-dimensional SBU, where ScO_6 octahedra

are connected by face-sharing carboxylate units, is found in [Sc_2BDC_3], where BDC = 1,4-benzenedicarboxylate,[36, 43] and an analogue linked by 1,4-naphthalenedicarboxylate.[44] These first five MOFs are all connected by the same BDC ligand, highlighting the need to carefully control reaction conditions such as time, temperature, and solvent, to select a desired phase.[40] An alternative approach to control phases is the use of modulated self-assembly, where additives such as monotopic analogues of the multitopic MOF ligand (coordination modulation) or mineral acids (pH modulation) can tune self-assembly kinetics and/or template specific SBUs to allow fine control over phase formation in complex systems.[45] Modulation has primarily been used to enhance and control physical properties such as crystallinity, defectivity, and porosity in MOFs linked by tetravalent metals such as Zr^{4+},[46-49] but emerging work suggests phase control is possible in MOFs linked by trivalent metals such as Al^{3+},[50] Fe^{3+},[51, 52] and Cr^{3+},[53] while modulation of Sc MOFs has been used to control porosity.[54]

Application of the isoreticular principle to MIL family MOFs has led to interpenetrated MIL-88 topology materials containing the discrete M_3O SBU,[51, 54-56] but catenated versions of MIL-53 topology MOFs with one-dimensional chain SBUs have not been reported to date. Indeed, it has been proposed that MOFs with such rod-like SBUs are highly unlikely to interpenetrate due to the short periodicity of the SBU – so-called "forbidden catenation"[57, 58] – but exceptions have been reported.[59] Herein, we report the modulated self-assembly of a two-fold interpenetrated Sc MOF with the MIL-53 topology, which we have named GUF-1 (Glasgow University Framework-1). Combining the extended 4,4′-(ethyne-1,2-diyl)dibenzoate (EDB^{2-}) ligand with the Sc-OH infinite chain SBU results in a MOF with limited flexibility compared to the archetypal MIL-53(Sc), which endows GUF-1 with permanent porosity. By using a combination of experiments and simulations, we confirm that a mixed-modulation strategy is essential to access samples with optimal porosity, where the combination of excellent uptake with a relatively dense material means GUF-1 provides excellent volumetric H_2 working capacities that are comparable to benchmark materials.

Results and Discussion

In the first instance, unmodulated solvothermal syntheses containing 4,4′-(ethyne-1,2-diyl)dibenzoic acid (EDB-H_2, prepared according to a modified literature procedure[60, 61]) and $Sc(NO_3)_3{\cdot}4H_2O$ in *N*,*N*-dimethylformamide (DMF) carried out at 100 ˚C resulted in a mixture of phases. Addition of hydrochloric acid (HCl) to a reaction mixture of EDB-H_2 and scandium nitrate in DMF that was heated at 100 ˚C for 24 hours yielded cuboidal single crystals of GUF-1 (see SI, Section S2). The MOF crystallises in the orthorhombic *Cmme* space group and has unit cell parameters of a = 7.3026(4) Å, b = 26.998(2) Å, c = 11.4979(8) Å. The structure of GUF-1-(HCl), named to denote the modulator used in its synthesis, consists of the characteristic one-dimensional chain, found in MIL-53(Sc)[39, 40]

and analogues, running down the crystallographic *a*-axis, where each metal is bridged by four carboxylate oxygen donors and two μ_2-OH linkers. Each EDB^{2-} linker binds to four separate scandium atoms, but its extended length results in a structure with two-fold interpenetration, where the one-dimensional Sc-OH chains of one net sit in the centre of the rhomboid channel of the other (Figure 1a). Interpenetration is facilitated by the alkyne spacer at the centre of the EDB^{2-} linker. The alkyne units of the interpenetrating nets stack upon one another, in an alternating fashion, at a distance of 3.65 Å apart from the centre of each alkyne bond (Figure 1b); we expect that steric hindrance would preclude a similar structure forming with a terphenylene-based linker, for example. This very small periodicity allows for interpenetration to occur, despite the one-dimensional chain SBU, which has a periodicity of ~7.3 Å, effectively locking the linkers together and limiting their movement relative to one another. Similar alkyne stacking has been observed in interpenetrated Zn MOFs of the EDB^{2-}[62] and 1,4-bis(1H-pyrazol-4-ylethynyl)benzene ligands.[59]

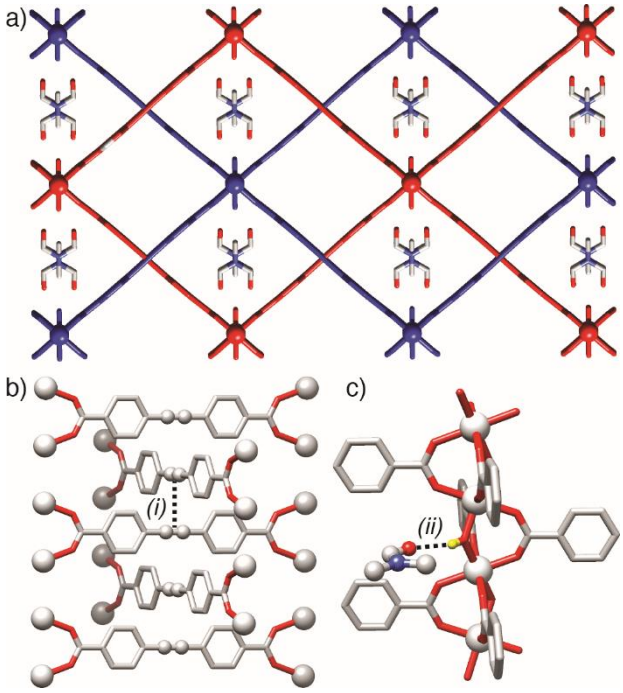

Figure 1. The crystal structure of GUF-1-(HCl). a) Crystal packing viewed down the crystallographic *a*-axis, showing the two interpenetrated nets, coloured red and blue, with disordered DMF solvent molecules in one of the two rhombic channels. b) Stacking of alkyne spacers (represented as spheres) of the EDB^{2-} linkers of adjacent nets, *(i)* = 3.65 Å (centroid to centroid). c) Hydrogen bonding between pore-bound DMF and bridging μ_2-OH, with positional disorder not shown, *(ii)* = 2.892(8) Å (O···O). Unless stated otherwise, C: grey; O: red; N: blue; H: yellow; Sc: Silver spheres. H atoms not involved in H bonding removed for clarity.

Two different rhombic channels form; one contains DMF solvent that could not be modelled, and the other is occupied by disordered DMF molecules that form hydrogen bonds with the μ_2-OH units that

project into the pore through the formamide oxygen (O···O = 2.892(8) Å, Figure 1c) to give an overall formula of [ScOH(EDB)]·DMF. To the best of our knowledge, this is the first report of an interpenetrated MIL-53 material – isoreticular analogues have been reported with the extended naphthalene-2,6-dicarboxylate[63, 64] and biphenyl-4,4′-dicarboxylate[64-68] linkers, but not for longer struts – and suggests that linkers with sterically small spacers, such as alkynes, could lead to interpenetrated phases in other systems linked by infinite 1D SBUs.[59]

The non-interpenetrated MIL-53(Sc), with BDC as linker, shows significant structural flexibility in the presence and absence of different guest molecules, with behaviour distinct from other homologues in the series.[39, 69] To investigate the impact of interpenetration on the flexibility of GUF-1, both single crystal and powder X-ray diffraction techniques were employed. In the first instance, simple solvent exchange of GUF-1-(HCl) crystals was carried out over 72 h at room temperature to determine if the pore-bound DMF could be exchanged and if differing solvation influences flexibility (see SI, Section S3). Breathing in MIL-53(Sc) occurs via hingeing motions around the metal-carboxylate bonding, "flattening" the rhombus-shaped channel, and resulting in a complex range of open, closed, and partially closed structures.[39, 69] In contrast, GUF-1-(HCl) shows distinct but minor changes when solvents are exchanged, which we have assessed by measuring angles Ψ and Φ, corresponding to the internal vertices of the rhombic pore, with a perfect square (Ψ = Φ = 90°) expected to represent the fully "open" structure (Figure 2a).

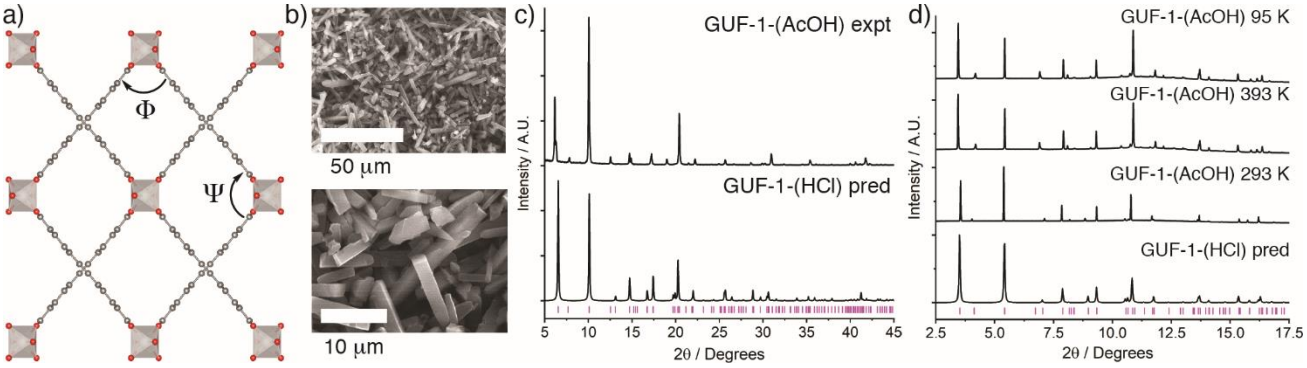

Figure 2. a) Schematic of pore vertice angles Ψ and Φ used to determine level of "openness" of GUF-1. b) Scanning electron micrographs of GUF-1-(AcOH) showing rod morphology. c) Powder X-ray diffractogram (flat plate, λ(CuKα) = 1.54183 Å) of GUF-1-(AcOH) compared to that predicted from the crystal structure of GUF-1-(HCl). d) Stacked powder-X-ray diffractograms (capillary, synchrotron radiation, E = 15 keV, λ = 0.826338 Å) of GUF-1-(AcOH) under vacuum at different temperatures compared to that predicted from the crystal structure of GUF-1-(HCl).

The "as-synthesised" DMF solvate, GUF-1-(HCl), has the most open form of the solvates examined

(Table 1). While single-crystal to single-crystal solvent exchange did change unit cell parameters, it was generally not possible to identify solvent in the pores, presumably due to disorder, but the loss of ordered DMF is suggestive of solvent exchange. Subtle changes are apparent after soaking in dichloromethane (CH_2Cl_2) and ethyl acetate (EtOAc). As the structure becomes more closed and the rhombic pore becomes more elongated, the *b*-axis increases, the *c*-axis decreases, and the unit cell volume decreases. The largest changes in unit cell parameters were found in the samples that were exchanged with 1,4-dioxane and isopropanol (^{i}PrOH); the *b*-axis increases by roughly 1.30 and 1.16 Å, respectively, coupled with a shortening in the *c*-axis by 0.87 and 0.71 Å. Quantitatively, going from the DMF solvate to the ^{i}PrOH solvate involves a unit cell volume contraction of 71.3 Å^3 (3.1%).

Table 1. Selected crystallographic data (150 K) for solvent exchanged single crystals of GUF-1-(HCl).

Solvent	a / Å	b / Å	c / Å	Volume / Å^3	Ψ / °[a]	Φ / °[a]
DMF[b]	7.3026 (4)	26.998 (2)	11.4979(8)	2266.88 (3)	99.2	80.8
CH_2Cl_2	7.3179 (4)	27.334 (1)	11.2728 (6)	2254.86 (2)	101.0	79.0
EtOAc	7.3142 (6)	27.545 (2)	11.189 (1)	2254.24 (3)	101.8	78.2
1,4-Dioxane	7.3050 (6)	28.157 (3)	10.7836 (9)	2218.46 (3)	105.1	74.9
^{i}PrOH	7.3033 (4)	28.300 (1)	10.6231 (6)	2195.60 (2)	106.2	73.8

[a]Angles Ψ and Φ correspond to the internal vertices of the rhombohedron shaped pore (see Figure 2a).

[b]The "as-synthesised" crystal structure of GUF-1-(HCl).

Bulk powder samples of GUF-1 can be synthesised (see SI, Section S2) by replacing HCl with acetic acid (AcOH) as modulator, to yield GUF-1-(AcOH) as micron-scale rod-shaped particles (Figure 2b). Samples were isolated by separating from the reaction solvent by centrifugation, followed by three acetone solvent exchanges and drying under reduced pressure in a vacuum dessicator, allowing for powder X-ray diffraction (PXRD) analysis to be carried out. GUF-1-(AcOH) shows a diffractogram similar to that predicted from the single crystal structure, but with minor differences suggesting potential flexibility on drying (Figure 2c). The position of Bragg reflections match the predicted diffraction pattern well, although relative intensities vary, which may be due to preferred orientation or minor changes in solvation (see SI, Section S4.1). To further examine the breathing of GUF-1 in the absence of guests, a bulk powder sample of GUF-1-(AcOH) was activated by washing in acetone three times and drying at 120 ˚C under vacuum (1.5×10^{-3} mbar for 24 hours on a rotary vane pump), and subsequently loaded into a capillary compatible with the gas cell[70] at the I11 beamline at Diamond Light Source.[71] Powder X-ray diffractograms (Figure 2d) were measured across a range of temperatures under vacuum, and Pawley fits used to assess the unit cell data (all diffractograms, fits, and unit cell data are provided in the SI, Section S4.2). At 298 K, V = 2277.1(1) Å^3, which correlates

closely to the DMF solvate crystal structure collected at 150 K (V = 2266.9(3) Å^3). The unit cell volume decreases slightly as the temperature is decreased (V = 2256.6(2) Å^3 at 95 K). After bringing the sample back to room temperature, a similar decrease in volume is observed upon subsequent heating (V = 2257.1(2) Å^3 at 393 K). This slight negative thermal expansion indicates the structure is closing and could be due either to the final removal of any residual solvent, or the increase in temperature facilitating additional flexibility. In any case, the volume changes are smaller than those observed by single-crystal X-ray diffraction upon solvent exchange, indicating host-guest interactions can influence the structure to a greater extent.

To assess the porosity of GUF-1 and the effect of synthesis modulator on physical properties, N_2 adsorption isotherms were carried at 77 K out on unmodulated (GUF-1) and AcOH modulated (GUF-1-(AcOH)) samples that had been activated by acetone washing and degassing (turbopump) at 150 °C for 20 h (Figure 3a). Both isotherms presented a small step around P/P_0 = 0.1 – this could be related either to stepwise pore-filling at different adsorption sites or the breathing phenomenon observed in flexible MOFs.[72, 73] In any case, GUF-1-(AcOH) showed a higher overall uptake (159 vs. 197 cm^3 (STP)/g at 1 bar for GUF-1 and GUF-1-(AcOH), respectively) and BET area (S_{BET} = 440 m^2 g^{-1} vs. 607 m^2 g^{-1} for GUF-1 and GUF-1-(AcOH), respectively). Comparison of PXRD data for GUF-1-(AcOH) before and after activation showed the appearance of some additional Bragg reflections, suggestive of possible flexibility or degradation (see SI, Figure S24).

As the unit cell volumes of evacuated samples were similar to the crystal structure of the DMF solvate (see SI, Table S1), the GUF-1-(HCl) crystal structure with pore-bound solvent omitted (denoted "as-synthesised", where Ψ = 99.2°, Φ = 80.8°) was used as the basis for grand canonical Monte Carlo (GCMC) simulations to assess the N_2 adsorption isotherm (see SI, Section S6). The simulation on a perfect and rigid structure predicts a much higher uptake of 274 cm^3 (STP)/g at 1 bar (Figure 3b) – it also showed a perfect Type I isotherm, which rejects the potential idea of stepwise filling of different adsorption sites, and suggests the observed step is indeed due to structure breathing. As such, a modified modulated self-assembly protocol was followed using L-proline (L-Pro), which has been shown previously to enhance crystallinity and porosity in Sc[54] and Zr[46, 47] MOFs. L-Proline was used as a co-modulator with AcOH to give GUF-1-(L-Pro/AcOH); after activation, the N_2 adsorption isotherm at 77 K showed a much higher uptake of 369 cm^3 (STP)/g (S_{BET} = 1080 m^2 g^{-1}) with narrow hysteresis. The isotherm also retained the step of the previous samples around P/P_0 = 0.1, which occurred at an N_2 uptake value of around 260 cm^3 (STP)/g, very close to the uptake capacity predicted by GCMC simulations for the as-synthesised structure, and suggesting the MOF is opening beyond what is seen in the GUF-1-(HCl) crystal structure. The ^{1}H NMR spectrum of an acid-digested sample

confirmed no L-proline, formylated proline, or DMF is retained in the pores (see SI, Figures S25 and S26), and suggests the MOF is fully activated and does not contain capping modulators as cluster-bound defects.

To probe this potential breathing, a fully "open" structure, where $\Psi = \Phi = 90^{\circ}$, was generated and an N_2 adsorption isotherm simulated. The predicted uptake of 372 cm^3 (STP)/g at 1 bar is again in excellent agreement with the experimental isotherm (Figure 3b), suggesting GUF-1-(L-Pro/AcOH) is fully activated and exhibits breathing at low partial pressures. Comparison of PXRD data for GUF-1-(L-Pro/AcOH) before and after isotherm collection showed no notable changes (Figure 3c), suggesting this breathing is reversible. GUF-1-(L-Pro/AcOH) therefore represents an example of a MOF with a potentially highly flexible topology wherein interpenetration likely limits this flexibility,[74] and ensures permanent porosity,[55] although we have not been able to prepare the non-interpenetrated analogue to confirm this.

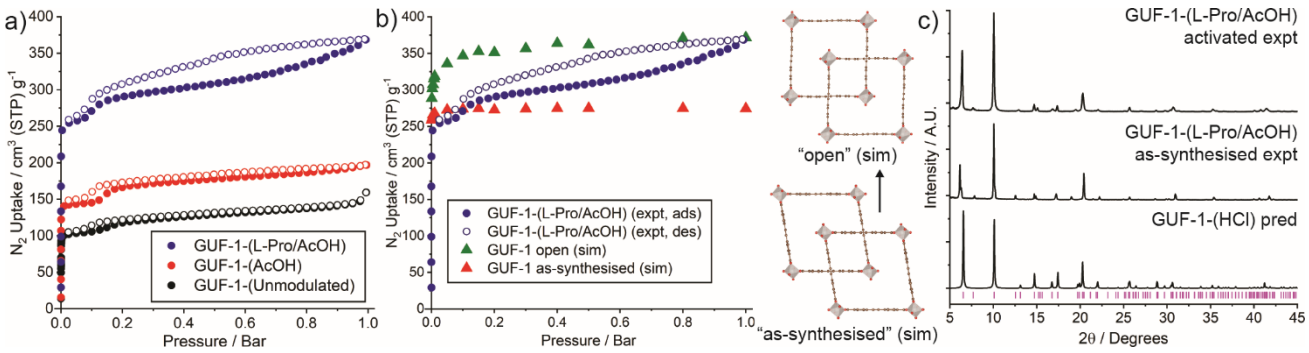

Figure 3. a) Comparison of N_2 adsorption/desorption isotherms (77 K) for GUF-1 samples prepared under different modulation conditions. b) Comparison of experimental N_2 adsorption (77 K) by GUF-1-(L-Pro/AcOH) with simulated isotherms for the "as-synthesised" ($\Psi = 99.2^{\circ}$, $\Phi = 80.8^{\circ}$) and "open" ($\Psi = \Phi = 90^{\circ}$) structural models, which are pictured c) Stacked powder X-ray diffractograms of GUF-1-(L-Pro/AcOH) before and after activation compared to the predicted diffractogram. The as-synthesised sample had been washed three times with acetone and dried under vacuum (desiccator) for 24 hours. The activated sample had been degassed at 150 C for 20 h and an N_2 adsorption/desorption isotherm collected at 77 K (one cycle).

Having optimised the synthetic conditions to access pristine MOF, a H_2 adsorption isotherm of GUF-1-(L-Pro/AcOH) was carried out at 77 K (Figure 4). Interestingly, the low subatmospheric H_2 isotherm, with an uptake of 287 cm^3 (STP)/g at 1 bar, shows the same narrow hysteresis as the N_2 adsorption isotherm; hysteresis in H_2 adsorption isotherms is not commonly observed in MOFs.[75, 76] This adsorption capacity for H_2 equates to 25.8 mg g^{-1}, or 2.52 wt%. GCMC simulations predicted uptakes of 247 and 288 cm^3 (STP)/g (2.18 and 2.52 wt%) at 1 bar for the as-synthesised and open

structures, respectively; the latter values are again very close to the experimental results and suggest GUF-1-(L-Pro/AcOH) breathes on exposure to H_2 at these partial pressures.

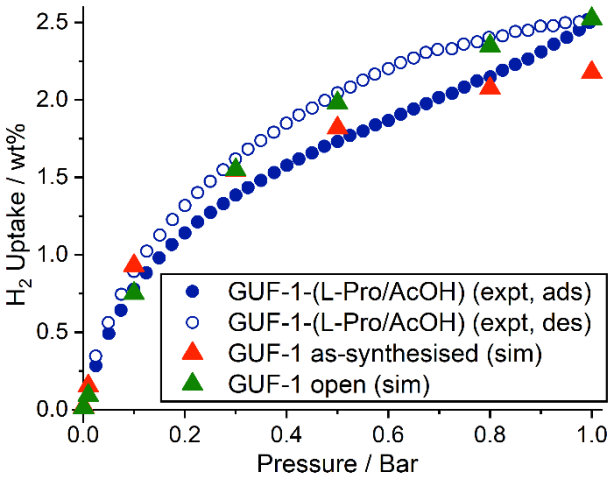

Figure 4. Experimental H_2 adsorption/desorption isotherm (77 K) for GUF-1-(L-Pro/AcOH) compared to simulated isotherms for the as-synthesised and open structural models of GUF-1.

To further probe the H_2 adsorption performance of GUF-1-(L-Pro/AcOH), high-pressure adsorption isotherms were run at two temperatures, 77 K and 160 K, and up to 110 bar (Figure 5a). It is important to note that the experimentally measured values are excess amounts adsorbed (N_{exc}), which are transformed into absolute uptakes (N_{abs}) by using equation (1):

$$N_{abs} = N_{exc} + \rho V_{pore} \quad (1)$$

where ρ is the density of the gas at the given adsorption pressure and temperature, obtained from the National Institute of Standards and Technology (NIST),[77] and V_{pore} is the pore volume of the adsorbent.[24] Similar to the adsorption of N_2, the H_2 isotherm at 77 K (Figure 5a) shows an interesting shape with two clear steps, evident from a dual-site Langmuir fitting (see SI, Figure S28), until it plateaus at ca. 80 bar with a volumetric uptake, based on the crystal density of the open structure, of 41.1 g L^{-1}. This could be indicative of further flexibility, induced by increased gas pressure, which has been observed in related systems.[72] Figure 5b shows the comparison of the experimental adsorption isotherm with the GCMC simulated ones for both the open and as-synthesised structural models of the material. The experimental isotherm at 77 K displayed similar saturation uptake (523 cm^3(STP)/g at 100 bar), to that simulated for the open structure material (543 cm^3(STP)/g at 100 bar), which suggests the larger pore volume of the open structure material enables enhanced H_2 adsorption performance at higher pressures.

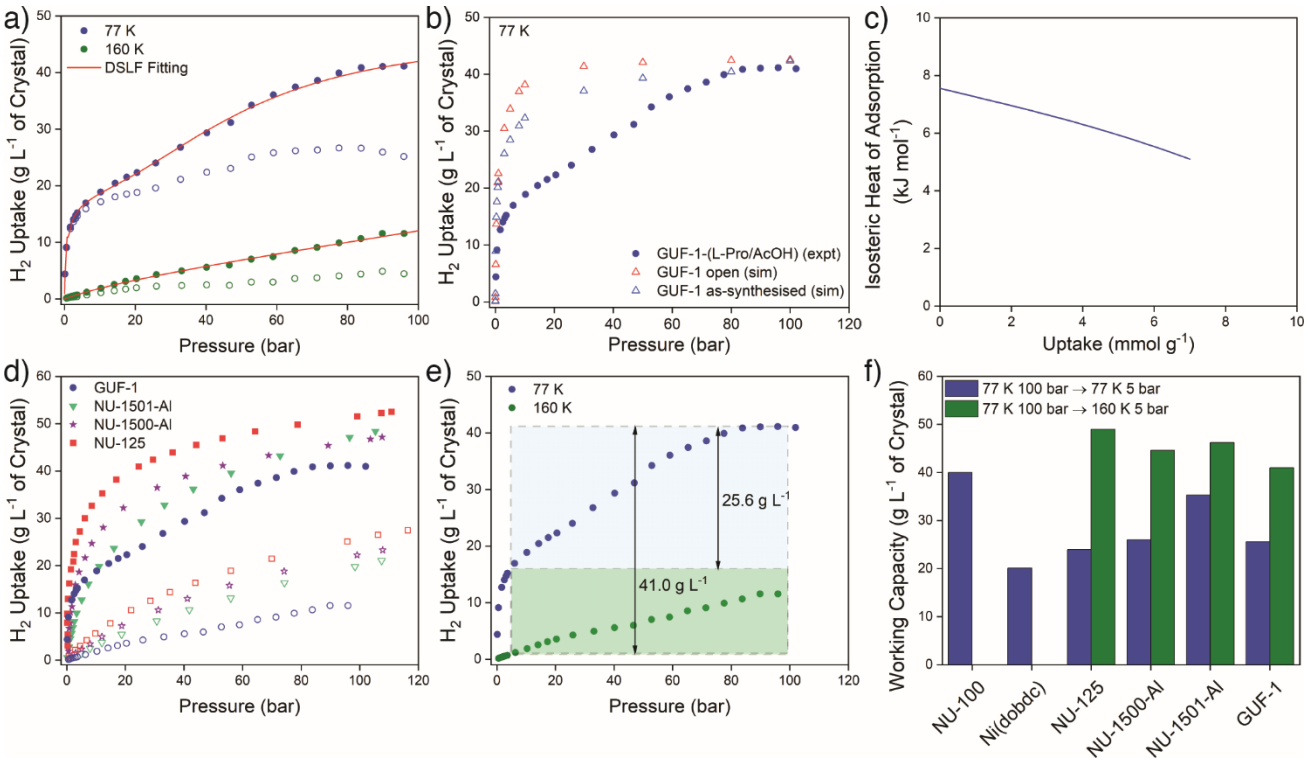

Figure 5. a) Volumetric H_2 adsorption for GUF-1-(L-Pro/AcOH) measured at 77 K and 160 K; absolute uptake is shown by closed symbols, while open symbols represent excess uptake. Absolute uptake values were calculated based upon an experimentally measured pore volume (at $P/P_0 = 0.99$) of 0.572 $cm^3\ g^{-1}$ and a crystal density of 0.878 g cm^{-3} for the open structure. b) Experimental high pressure absolute H_2 isotherm compared to GCMC calculated H_2 uptake for the open and as-synthesised structures for GUF-1-(L-Pro/AcOH). c) Isosteric heat of adsorption (Q_{st}) for H_2 adsorption on GUF-1-(L-Pro/AcOH) calculated using the Virial method and H_2 isotherms at 77 K and 160 K. d) H_2 adsorption isotherms (77 K and 160 K) of GUF-1-(L-Pro/AcOH) and benchmark MOFs; closed symbols represent 77 K experiments, open symbols represent 160 K experiments. e**)** Cryogenic H_2 gas delivery for pressure swing (100 bar/77 K → 5 bar/77 K) and temperature-pressure swing (100 bar/77 K → 5 bar/160 K) storage systems for GUF-1-(L-Pro/AcOH). f) H_2 working capacity of GUF-1-(L-Pro/AcOH) compared to benchmark materials (data replotted from corresponding publications for NU-100,[9] NU-125,[8] Ni(dobdc),[10] NU-1500-Al,[11] and NU-1501-Al[11] and tabulated in the SI, Table S4).

Interestingly, GUF-1-(L-Pro/AcOH) displays an exceptional high H_2 uptake in the low-pressure region (0-2 bar), which suggests high adsorbent-adsorbate interaction energy between the MOF and H_2 gas. We used the Virial method to estimate the isosteric heat of adsorption (Q_{st}) using the H_2 isotherms collected at 77 and 160 K (Figure 5c). The experimental Q_{st} at low coverage for GUF-1-(L-Pro/AcOH) was *ca.* 7.6 kJ mol^{-1}, which exceeds those for many previously reported high capacity benchmark adsorbents (see SI, Table S4), although higher values can been obtained by narrow-pore materials[78-80] or those with open metal sites.[81, 82] This high Q_{st} for H_2 can be attributed to the narrow

porosity of the closed structure and strong π-π interactions between H_2 and the aromatic rings of the linker ligands of the GUF-1-(L-Pro/AcOH) framework.

MOFs generally display Type I isotherms for adsorption of H_2 under cryogenic conditions, with high loadings at low pressures, followed by a saturation of the H_2 uptake at higher ones. This limits the overall working capacity of the adsorbent materials.[5] To address this issue, the DoE Hydrogen Storage Engineering Center of Excellence (HSECoE) has proposed designing tanks for cryo-adsorption storage that operate with H_2 loading occurring at 77 K and 100 bar and discharge occurring at 160 K and 5 bar, ensuring the amount of deliverable H_2 in nanoporous MOFs is maximised.[10] In this way, we examined the material for use in cryogenic H_2 gas delivery for pressure swing (100 bar and 77 K → 5 bar and 77 K) and temperature-pressure swing (100 bar and 77 K → 5 bar and 160 K) systems. For the purposes of this study, we limited our analysis to benchmark materials whose H_2 adsorption performance was based on crystal structure densities. Figure 5d shows the comparison of the uptake of GUF-1-(L-Pro/AcOH) at 77 K with benchmark materials; GUF-1-(L-Pro/AcOH) exhibits slightly lower H_2 uptake to that of NU-1501 and NU-1500, with NU-100 and Ni(dobdc) outperforming GUF-1-(L-Pro/AcOH) at higher pressures (see SI, Table S4). Calculating the working capacity for a cryogenic pressure swing (100 bar and 77 K → 5 bar and 77 K) system (Figure 5e), GUF-1-(L-Pro/AcOH), however, outperforms Ni(dobdc) by delivering *ca.* 26 g L^{-1} H_2 between 100 and 5 bar (Figure 5f). For a combined temperature-pressure swing (100 bar and 77 K → 5 bar and 160 K) system (Figure 5e), GUF-1-(L-Pro/AcOH) displayed a working capacity of *ca.* 41 g L^{-1}. This was found to be comparable to the previously reported benchmark materials examined under similar conditions (Figure 5f). Despite the slightly lower H_2 uptake at 77 K compared to the current benchmarks such as NU-125,[8] NU-1500,[11] and NU-1501[11] (Figure 5d), the significantly lower H_2 uptake at 160 K enables GUF-1-(L-Pro/AcOH) to maximise the H_2 delivered in a combined temperature-pressure swing system, illustrating its great potential for use H_2 storage applications.

Conclusions

By using a carefully controlled self-assembly strategy and a reticular chemistry approach, we have reported an unusual example of an interpenetrated MIL-53 topology MOF, which has limited flexibility due to catenation but maintains permanent porosity. By using a sterically unhindered spacer at the centre of the EDB^{2-} linker, close stacking of adjacent nets with low periodicity (3.65 Å) facilitates interpenetration, even with an infinite rod SBU. The full porosity of GUF-1-(L-Pro/AcOH) has been accessed by a combination of GCMC simulations and bespoke coordination modulation experiments, leading to a material with an excellent working capacity for H_2 storage and delivery in a combined temperature-pressure swing system. The work shows the importance of coordination

modulation in both the discovery and optimisation of MOFs, while GUF-1-(L-Pro/AcOH) stands as an example of a material constructed from relatively simple building blocks that can still exhibit a highly desirable uptake and working capacity for hydrogen storage applications.

Acknowledgements

R.S.F. thanks the Royal Society for receipt of a URF and the University of Glasgow for funding. The work has been supported in part by EPSRC (EP/L004461/1, EP/N509668/1) and the European Research Council (ERC) under the European Union's Horizon 2020 Programme for Research and Innovation (grant agreement no. 677289, SCoTMOF, ERC-2015-STG). S.A.M. thanks the Australian Research Council (ARC) for a Future Fellowship (FT200100243). G.F.T. acknowledges the Australian Government for the provision of an RTP scholarship. D.F.-J. thanks the Royal Society for receipt of a URF, the European Research Council (ERC) under the European Union's Horizon 2020 research and innovation programme (NanoMOFdeli), ERC-2016-COG 726380, Innovate UK (104384) and EPSRC IAA (IAA/RG85685). We acknowledge Diamond Light Source for time on I11 under proposal CY22028.

References

1. H. Furukawa, K. E. Cordova, M. O'Keeffe and O. M. Yaghi, *Science*, 2013, **341**, 1230444.
2. K. Sumida, D. L. Rogow, J. A. Mason, T. M. McDonald, E. D. Bloch, Z. R. Herm, T.-H. Bae and J. R. Long, *Chem. Rev.*, 2012, **112**, 724-781.
3. E. Barea, C. Montoro and J. A. R. Navarro, *Chem. Soc. Rev.*, 2014, **43**, 5419-5430.
4. J.-R. Li, R. J. Kuppler and H.-C. Zhou, *Chem. Soc. Rev.*, 2009, **38**, 1477-1504.
5. B. M. Connolly, D. G. Madden, A. E. H. Wheatley and D. Fairen-Jimenez, *J. Am. Chem. Soc.*, 2020, **142**, 8541-8549.
6. H. Li, K. Wang, Y. Sun, C. T. Lollar, J. Li and H.-C. Zhou, *Mater. Today*, 2018, **21**, 108-121.
7. T. Tian, Z. Zeng, D. Vulpe, M. E. Casco, G. Divitini, P. A. Midgley, J. Silvestre-Albero, J.-C. Tan, P. Z. Moghadam and D. Fairen-Jimenez, *Nat. Mater.*, 2018, **17**, 174-179.
8. P. García-Holley, B. Schweitzer, T. Islamoglu, Y. Liu, L. Lin, S. Rodriguez, M. H. Weston, J. T. Hupp, D. A. Gómez-Gualdrón, T. Yildirim and O. K. Farha, *ACS Energy Lett.*, 2018, **3**, 748-754.
9. O. K. Farha, A. Özgür Yazaydın, I. Eryazici, C. D. Malliakas, B. G. Hauser, M. G. Kanatzidis, S. T. Nguyen, R. Q. Snurr and J. T. Hupp, *Nature Chem.*, 2010, **2**, 944-948.
10. M. T. Kapelewski, T. Runčevski, J. D. Tarver, H. Z. H. Jiang, K. E. Hurst, P. A. Parilla, A. Ayala, T. Gennett, S. A. FitzGerald, C. M. Brown and J. R. Long, *Chem. Mater.*, 2018, **30**, 8179-8189.

11. Z. Chen, P. Li, R. Anderson, X. Wang, X. Zhang, L. Robison, L. R. Redfern, S. Moribe, T. Islamoglu, D. A. Gómez-Gualdrón, T. Yildirim, J. F. Stoddart and O. K. Farha, *Science*, 2020, **368**, 297.
12. D. A. Gómez-Gualdrón, T. C. Wang, P. García-Holley, R. M. Sawelewa, E. Argueta, R. Q. Snurr, J. T. Hupp, T. Yildirim and O. K. Farha, *ACS Appl. Mater. Interfaces*, 2017, **9**, 33419-33428.
13. M. P. Suh, H. J. Park, T. K. Prasad and D.-W. Lim, *Chem. Rev.*, 2012, **112**, 782-835.
14. M. D. Allendorf, Z. Hulvey, T. Gennett, A. Ahmed, T. Autrey, J. Camp, E. Seon Cho, H. Furukawa, M. Haranczyk, M. Head-Gordon, S. Jeong, A. Karkamkar, D.-J. Liu, J. R. Long, K. R. Meihaus, I. H. Nayyar, R. Nazarov, D. J. Siegel, V. Stavila, J. J. Urban, S. P. Veccham and B. C. Wood, *Energy Environ. Sci.*, 2018, **11**, 2784-2812.
15. S. P. Shet, S. Shanmuga Priya, K. Sudhakar and M. Tahir, *Int. J. Hydrog. Energy*, 2021, **46**, 11782-11803.
16. O. M. Yaghi, M. O'Keeffe, N. W. Ockwig, H. K. Chae, M. Eddaoudi and J. Kim, *Nature*, 2003, **423**, 705-714.
17. W. Fan, X. Zhang, Z. Kang, X. Liu and D. Sun, *Coord. Chem. Rev.*, 2021, **443**, 213968.
18. Y.-N. Gong, D.-C. Zhong and T.-B. Lu, *CrystEngComm*, 2016, **18**, 2596-2606.
19. H.-L. Jiang, T. A. Makal and H.-C. Zhou, *Coord. Chem. Rev.*, 2013, **257**, 2232-2249.
20. G.-P. Yang, L. Hou, L.-F. Ma and Y.-Y. Wang, *CrystEngComm*, 2013, **15**, 2561-2578.
21. G. Verma, S. Butikofer, S. Kumar and S. Ma, *Top. Curr. Chem.*, 2020, **378**, 4.
22. H. Deng, S. Grunder, K. E. Cordova, C. Valente, H. Furukawa, M. Hmadeh, F. Gándara, A. C. Whalley, Z. Liu, S. Asahina, H. Kazumori, M. O'Keeffe, O. Terasaki, J. F. Stoddart and O. M. Yaghi, *Science*, 2012, **336**, 1018.
23. O. Shekhah, H. Wang, M. Paradinas, C. Ocal, B. Schüpbach, A. Terfort, D. Zacher, R. A. Fischer and C. Wöll, *Nat. Mater.*, 2009, **8**, 481-484.
24. D. Fairen-Jimenez, Y. J. Colón, O. K. Farha, Y.-S. Bae, J. T. Hupp and R. Q. Snurr, *Chem. Commun.*, 2012, **48**, 10496-10498.
25. J. Goldsmith, A. G. Wong-Foy, M. J. Cafarella and D. J. Siegel, *Chem. Mater.*, 2013, **25**, 3373-3382.
26. A. Ahmed, Y. Liu, J. Purewal, L. D. Tran, A. G. Wong-Foy, M. Veenstra, A. J. Matzger and D. J. Siegel, *Energy Environ. Sci.*, 2017, **10**, 2459-2471.
27. D. P. Broom, C. J. Webb, G. S. Fanourgakis, G. E. Froudakis, P. N. Trikalitis and M. Hirscher, *Int. J. Hydrog. Energy*, 2019, **44**, 7768-7779.
28. P. Nugent, Y. Belmabkhout, S. D. Burd, A. J. Cairns, R. Luebke, K. Forrest, T. Pham, S. Ma, B. Space, L. Wojtas, M. Eddaoudi and M. J. Zaworotko, *Nature*, 2013, **495**, 80-84.

29. M. Dincă, A. Dailly, C. Tsay and J. R. Long, *Inorg. Chem.*, 2008, **47**, 11-13.
30. J. L. C. Rowsell and O. M. Yaghi, *Angew. Chem. Int. Ed.*, 2005, **44**, 4670-4679.
31. P. L. Llewellyn, S. Bourrelly, C. Serre, Y. Filinchuk and G. Férey, *Angew. Chem. Int. Ed.*, 2006, **45**, 7751-7754.
32. M. Latroche, S. Surblé, C. Serre, C. Mellot-Draznieks, P. L. Llewellyn, J.-H. Lee, J.-S. Chang, S. H. Jhung and G. Férey, *Angew. Chem. Int. Ed.*, 2006, **45**, 8227-8231.
33. L. Hamon, C. Serre, T. Devic, T. Loiseau, F. Millange, G. Férey and G. D. Weireld, *J. Am. Chem. Soc.*, 2009, **131**, 8775-8777.
34. P. Z. Moghadam, A. Li, X.-W. Liu, R. Bueno-Perez, S.-D. Wang, S. B. Wiggin, P. A. Wood and D. Fairen-Jimenez, *Chem. Sci.*, 2020, **11**, 8373-8387.
35. I. A. Ibarra, X. Lin, S. Yang, A. J. Blake, G. S. Walker, S. A. Barnett, D. R. Allan, N. R. Champness, P. Hubberstey and M. Schröder, *Chem. Eur. J.*, 2010, **16**, 13671-13679.
36. J. Perles, M. Iglesias, M.-Á. Martín-Luengo, M. Á. Monge, C. Ruiz-Valero and N. Snejko, *Chem. Mater.*, 2005, **17**, 5837-5842.
37. I. A. Ibarra, S. Yang, X. Lin, A. J. Blake, P. J. Rizkallah, H. Nowell, D. R. Allan, N. R. Champness, P. Hubberstey and M. Schröder, *Chem. Commun.*, 2011, **47**, 8304-8306.
38. C. O. Areán, C. P. Cabello and G. T. Palomino, *Chem. Phys. Lett.*, 2012, **521**, 104-106.
39. J. P. S. Mowat, V. R. Seymour, J. M. Griffin, S. P. Thompson, A. M. Z. Slawin, D. Fairen-Jimenez, T. Düren, S. E. Ashbrook and P. A. Wright, *Dalton Trans.*, 2012, **41**, 3937-3941.
40. J. P. S. Mowat, S. R. Miller, A. M. Z. Slawin, V. R. Seymour, S. E. Ashbrook and P. A. Wright, *Microporous Mesoporous Mater.*, 2011, **142**, 322-333.
41. L. Mitchell, B. Gonzalez-Santiago, J. P. S. Mowat, M. E. Gunn, P. Williamson, N. Acerbi, M. L. Clarke and P. A. Wright, *Catal. Sci. Technol.*, 2013, **3**, 606-617.
42. P. D. C. Dietzel, R. Blom and H. Fjellvåg, *Dalton Trans.*, 2006, 2055-2057.
43. S. R. Miller, P. A. Wright, C. Serre, T. Loiseau, J. Marrot and G. Férey, *Chem. Commun.*, 2005, 3850-3852.
44. P. Rönfeldt, H. Reinsch, E. Svensson Grape, A. K. Inge, H. Terraschke and N. Stock, *Z. Anorg. Allg. Chem.*, 2020, **646**, 1373-1379.
45. R. S. Forgan, *Chem. Sci.*, 2020, **11**, 4546-4562.
46. O. V. Gutov, S. Molina, E. C. Escudero-Adán and A. Shafir, *Chem. Eur. J.*, 2016, **22**, 13582-13587.
47. R. J. Marshall, C. L. Hobday, C. F. Murphie, S. L. Griffin, C. A. Morrison, S. A. Moggach and R. S. Forgan, *J. Mater. Chem. A*, 2016, **4**, 6955-6963.
48. A. Schaate, P. Roy, A. Godt, J. Lippke, F. Waltz, M. Wiebcke and P. Behrens, *Chem. Eur. J.*, 2011, **17**, 6643-6651.

49. Y. Bai, Y. Dou, L.-H. Xie, W. Rutledge, J.-R. Li and H.-C. Zhou, *Chem. Soc. Rev.*, 2016, **45**, 2327-2367.
50. F. J. Carmona, C. R. Maldonado, S. Ikemura, C. C. Romão, Z. Huang, H. Xu, X. Zou, S. Kitagawa, S. Furukawa and E. Barea, *ACS Appl. Mater. Interfaces*, 2018, **10**, 31158-31167.
51. D. Bara, C. Wilson, M. Mörtel, M. M. Khusniyarov, S. Ling, B. Slater, S. Sproules and R. S. Forgan, *J. Am. Chem. Soc.*, 2019, **141**, 8346-8357.
52. D. Bara, E. Meekel, I. Pakamore, C. Wilson, S. Ling and R. S. Forgan, *Mater. Horiz.*, 2021, DOI: 10.1039/D1MH01663F.
53. L. Yang, T. Zhao, I. Boldog, C. Janiak, X.-Y. Yang, Q. Li, Y.-J. Zhou, Y. Xia, D.-W. Lai and Y.-J. Liu, *Dalton Trans.*, 2019, **48**, 989-996.
54. R. J. Marshall, C. T. Lennon, A. Tao, H. M. Senn, C. Wilson, D. Fairen-Jimenez and R. S. Forgan, *J. Mater. Chem. A*, 2018, **6**, 1181-1187.
55. M. Dan-Hardi, H. Chevreau, T. Devic, P. Horcajada, G. Maurin, G. Férey, D. Popov, C. Riekel, S. Wuttke, J.-C. Lavalley, A. Vimont, T. Boudewijns, D. de Vos and C. Serre, *Chem. Mater.*, 2012, **24**, 2486-2492.
56. D. Feng, K. Wang, Z. Wei, Y.-P. Chen, C. M. Simon, R. K. Arvapally, R. L. Martin, M. Bosch, T.-F. Liu, S. Fordham, D. Yuan, M. A. Omary, M. Haranczyk, B. Smit and H.-C. Zhou, *Nat. Commun.*, 2014, **5**, 5723.
57. N. L. Rosi, M. Eddaoudi, J. Kim, M. O'Keeffe and O. M. Yaghi, *Angew. Chem. Int. Ed.*, 2002, **41**, 284-287.
58. A. Schoedel, M. Li, D. Li, M. O'Keeffe and O. M. Yaghi, *Chem. Rev.*, 2016, **116**, 12466-12535.
59. S. Galli, A. Maspero, C. Giacobbe, G. Palmisano, L. Nardo, A. Comotti, I. Bassanetti, P. Sozzani and N. Masciocchi, *J. Mater. Chem. A*, 2014, **2**, 12208-12221.
60. T. Gadzikwa, B.-S. Zeng, J. T. Hupp and S. T. Nguyen, *Chem. Commun.*, 2008, 3672-3674.
61. R. J. Marshall, S. L. Griffin, C. Wilson and R. S. Forgan, *J. Am. Chem. Soc.*, 2015, **137**, 9527-9530.
62. D. J. Tranchemontagne, K. S. Park, H. Furukawa, J. Eckert, C. B. Knobler and O. M. Yaghi, *J. Phys. Chem. C*, 2012, **116**, 13143-13151.
63. T. Loiseau, C. Mellot-Draznieks, H. Muguerra, G. Férey, M. Haouas and F. Taulelle, *Compt. Rend. Chim.*, 2005, **8**, 765-772.
64. I. Senkovska, F. Hoffmann, M. Fröba, J. Getzschmann, W. Böhlmann and S. Kaskel, *Microporous Mesoporous Mater.*, 2009, **122**, 93-98.

65. Y.-Y. Liu, S. Couck, M. Vandichel, M. Grzywa, K. Leus, S. Biswas, D. Volkmer, J. Gascon, F. Kapteijn, J. F. M. Denayer, M. Waroquier, V. Van Speybroeck and P. Van Der Voort, *Inorg. Chem.*, 2013, **52**, 113-120.
66. Y.-Y. Liu, R. Decadt, T. Bogaerts, K. Hemelsoet, A. M. Kaczmarek, D. Poelman, M. Waroquier, V. Van Speybroeck, R. Van Deun and P. Van Der Voort, *J. Phys. Chem. C*, 2013, **117**, 11302-11310.
67. E. D. Bloch, D. Britt, C. Lee, C. J. Doonan, F. J. Uribe-Romo, H. Furukawa, J. R. Long and O. M. Yaghi, *J. Am. Chem. Soc.*, 2010, **132**, 14382-14384.
68. P. Rönfeldt, N. Ruser, H. Reinsch, E. S. Grape, A. Ken Inge, M. Suta, H. Terraschke and N. Stock, *Eur. J. Inorg. Chem.*, 2020, **2020**, 2737-2743.
69. L. Chen, J. P. S. Mowat, D. Fairen-Jimenez, C. A. Morrison, S. P. Thompson, P. A. Wright and T. Düren, *J. Am. Chem. Soc.*, 2013, **135**, 15763-15773.
70. J. E. Parker, J. Potter, S. P. Thompson, A. R. Lennie and C. C. Tang, *Mater. Sci. Forum*, 2012, **706-709**, 1707-1712.
71. S. P. Thompson, J. E. Parker, J. Marchal, J. Potter, A. Birt, F. Yuan, R. D. Fearn, A. R. Lennie, S. R. Street and C. C. Tang, *J. Synchrotron Radiat.*, 2011, **18**, 637-648.
72. C. Serre, S. Bourrelly, A. Vimont, N. A. Ramsahye, G. Maurin, P. L. Llewellyn, M. Daturi, Y. Filinchuk, O. Leynaud, P. Barnes and G. Férey, *Adv. Mater.*, 2007, **19**, 2246-2251.
73. E. J. Carrington, C. A. McAnally, A. J. Fletcher, S. P. Thompson, M. Warren and L. Brammer, *Nature Chem.*, 2017, **9**, 882-889.
74. M. Vicent-Morales, I. J. Vitórica-Yrezábal, M. Souto and G. Mínguez Espallargas, *CrystEngComm*, 2019, **21**, 3031-3035.
75. H. J. Park and M. P. Suh, *Chem. Commun.*, 2010, **46**, 610-612.
76. H. J. Choi, M. Dincă and J. R. Long, *J. Am. Chem. Soc.*, 2008, **130**, 7848-7850.
77. E. W. Lemmon, M. O. McLinden and D. G. Friend, in *NIST Standard Reference Database Number 69*, eds. P. J. Lindstrom and W. G. Mallard, National Institute of Standards and Technology, 2016, DOI: https://doi.org/10.18434/T4D303.
78. K. A. Forrest, T. Pham, P. A. Georgiev, F. Pinzan, C. R. Cioce, T. Unruh, J. Eckert and B. Space, *Langmuir*, 2015, **31**, 7328-7336.
79. M. H. Alkordi, Y. Belmabkhout, A. Cairns and M. Eddaoudi, *IUCrJ*, 2017, **4**, 131-135.
80. P. Nugent, T. Pham, K. McLaughlin, P. A. Georgiev, W. Lohstroh, J. P. Embs, M. J. Zaworotko, B. Space and J. Eckert, *J. Mater. Chem. A*, 2014, **2**, 13884-13891.
81. P. D. C. Dietzel, P. A. Georgiev, J. Eckert, R. Blom, T. Strässle and T. Unruh, *Chem. Commun.*, 2010, **46**, 4962-4964.

82. J. G. Vitillo, L. Regli, S. Chavan, G. Ricchiardi, G. Spoto, P. D. C. Dietzel, S. Bordiga and A. Zecchina, *J. Am. Chem. Soc.*, 2008, **130**, 8386-8396.